Toxicology and Applied Pharmacology 393 (2020) 114955

Contents lists available at ScienceDirect

Toxicology and Applied Pharmacology

journal homepage: www.elsevier.com/locate/taap

Demyelination associated with chronic arsenic exposure in Wistar rats

Sandra A. Niño[a], Erika Chi-Ahumada[b], Juan Ortíz[c], Sergio Zarazua[a], Luis Concha[c], Maria E. Jiménez-Capdeville[b,*]

[a] Laboratorio de Neurotoxicología, Facultad de Ciencias Químicas, Universidad Autónoma de San Luis Potosí, Av. Manuel Nava 6, C.P 78210 San Luis Potosí, Mexico
[b] Departamento de Bioquímica, Facultad de Medicina, Universidad Autónoma de San Luis Potosí, Av. Venustiano Carranza 2405, C.P 78210 San Luis Potosí, Mexico
[c] Instituto de Neurobiología, Universidad Nacional Autónoma de México, Boulevard Juriquilla 3001, Querétaro, Querétaro C.P 76230, Mexico

ARTICLE INFO

Keywords:
Demyelination
Arsenic
Development
Axonal damage
Amyloid
Mitochondria
Microstructure
DTI
Anisotropy
MRI

ABSTRACT

Inorganic arsenic is among the major contaminants of groundwater in the world. Worldwide population-based studies demonstrate that chronic arsenic exposure is associated with poor cognitive performance among children and adults, while research in animal models confirms learning and memory deficits after arsenic exposure. The aim of this study was to investigate the long-term effects of environmentally relevant arsenic exposure in the myelination process of the prefrontal cortex (PFC) and corpus callosum (CC). A longitudinal study with repeated follow-up assessments was performed in male Wistar rats exposed to 3 ppm sodium arsenite in drinking water. Animals received the treatment from gestation until 2, 4, 6, or 12 months of postnatal age. The levels of myelin basic protein (MBP) were evaluated by immunohistochemistry/histology and immunoblotting from the PFC and CC. As plausible alterations associated with demyelination, we considered mitochondrial mass (VDAC) and two axonal damage markers: amyloid precursor protein (APP) level and phosphorylated neurofilaments. To analyze the microstructure of the CC *in vivo*, we acquired diffusion-weighted images at the same ages, from which we derived metrics using the tensor model. Significantly decreased levels of MBP were found in both regions together with significant increases of mitochondrial mass and slight axonal damage at 12 months in the PFC. Ultrastructural imaging demonstrated arsenic-associated decreases of white matter volume, water diffusion anisotropy, and increases in radial diffusivity. This study indicates that arsenic exposure is associated with a significant and persistent negative impact on microstructural features of white matter tracts.

1. Introduction

Myelination of axons is one of the main processes that shape brain structural and functional maturation throughout life. Developmental myelination is a complex but orderly process that occurs in predictable topographical and chronological sequences (Andersen, 2003). The multilamellar extension of membrane from oligodendrocytes, which wraps around axons, enhances the propagation of action potentials and is therefore essential for the proper function of neural circuits (Barkovich, 2000). Myelination is also an important form of brain plasticity since it is modifiable by experience (Mount and Monje, 2017) and environmental factors, especially early in life, but continuing until the fourth decade in humans (Lebel et al., 2012). Consequently, abnormal myelination or pathological loss of myelin can lead to a severe loss of function including motor and sensory dysfunction (McKenzie et al., 2014), neurobehavioral and cognitive impairments, psychiatric disorders (Paus et al., 2008; Takahashi et al., 2011), and neurodegeneration (Nasrabady et al., 2018).

Over the past decades, interactions between psychosocial, genetic, and environmental factors that may modify white matter have been extensively investigated. Abundant literature demonstrates that environmental toxicants such as arsenic interfere with brain plasticity, disturbing cognitive processes; however, direct evidence of their effect on myelination is scarce (Cabral-Pinto et al., 2018). Poor cognition, decreased visuospatial skills, affected memory and attention, as well as mood disorders, have been reported as consequences of human arsenic exposure in the pediatric population (Calderón et al., 2001; Wasserman et al., 2014), through adolescence and adulthood (Tsai et al., 2003), and in geriatric patients (O'Bryant et al., 2011). This neurological impact attracts attention because arsenic is considered one of the most hazardous chemicals to which millions of people are exposed worldwide, mainly through its presence in groundwater (WHO, 2016). Alterations induced by arsenic at different levels of neural signaling that may underlie cognitive deficits have been demonstrated *in vivo* and *in vitro* (Tyler and Allan, 2014), and some studies have specifically addressed myelination in animals.

* Corresponding author at: Departamento de Bioquímica, Facultad de Medicina, UASLP, Av. Venustiano Carranza 2405, San Luis Potosí, Mexico.
E-mail address: mejimenez@uaslp.mx (M.E. Jiménez-Capdeville).

https://doi.org/10.1016/j.taap.2020.114955
Received 1 January 2020; Received in revised form 18 February 2020; Accepted 10 March 2020
Available online 14 March 2020
0041-008X/ © 2020 Elsevier Inc. All rights reserved.

Toxic effects induced by inorganic arsenic have been demonstrated in myelinated nerve fibers of prefrontal cortex (PFC), optic nerve, and retina of the rat (Rai et al., 2013), and in the fibers of the striatum (Zarazúa et al., 2010; Ríos et al., 2012). These studies do not disclose, however, whether myelin alterations are taking place in parallel with axonal damage. At environmentally relevant exposure levels, arsenic impairs energy generation required for axonal transport and alters the expression of neurofilaments in cell cultures (Aung et al., 2013a; Chandravanshi et al., 2018). Exposed rats show accumulation of amyloid precursor protein (APP), which is a marker of impaired axonal transport, and oxidative damage has been reported in neural membranes (Niño et al., 2018). It is therefore plausible that both axons and myelin are targets of arsenic exposure.

As a form of plasticity contributing to cognitive processes, myelination requires a closer analysis under arsenic exposure. By combining imaging techniques and histological assessments, microstructural changes can be evaluated in key structures related to cognitive performance. Among them, the corpus callosum (CC) contains axonal fibers that mediate interhemispheric transfer of information across the PFC. Researchers have proposed, based on the large amounts of information transferred back and forth between the two hemispheres *via* the CC, that the degeneration of white matter architecture or "structural disconnection" could be one of the key factors underlying the cognitive decline associated with arsenic (Raz and Rodrigue, 2006). Therefore, the aim of this study was to investigate the long-term effects of environmentally relevant arsenic exposure in the myelination process of the PFC and CC.

The rat model of arsenic exposure resembles human developmental exposure. In this model, rats are exposed to arsenic from gestation to 4 months of age through drinking water (approximately 0.4 mg/kg/day), first to the dams and continuing after weaning. In this model, neurochemical, epigenetic and behavioral alterations have been previously demonstrated (Martínez et al., 2011; Zarazúa et al., 2006). Also, similar doses of arsenic result in alterations of synapse structure, impaired learning, and long- and short-term memory, evaluated through performance in the Y maze and Morris water maze (Jing et al., 2012; Luo et al., 2009). The Wistar rat is best suited to analyze the possible arsenic effects on myelination, since every developmental myelin stage is well characterized (Bockhorst et al., 2008). Briefly, axons at 5 postnatal days (PND) are in a "pre-myelinating" state (Prayer et al., 2001), whereby axonal electrical activity increases the production or release of growth factors responsible for the proliferation of oligodendrocyte precursor cells (Miller, 2002). After reaching a maximal rate of myelin accumulation near PND 20 (Downes and Mullins, 2014), central structures show nearly complete myelination around PND 24, and the process follows the volume and cell number changes that the rat brain experiences until the third month (Markham et al., 2007; Willing and Juraska, 2015). From 3 to 12 months of age myelin content remains stable, although myelination continues in the PFC, followed by an age-related decline afterwards (Mengler et al., 2014; Wang et al., 2020). At 2 and 3 months of age, white matter volume is higher in male than in female rats, but no available data indicate whether this tendency persists at older age (Willing and Juraska, 2015). According to this background, 2-, 4- and 6-month-old male animals were studied, since the major period of myelination of white matter tracts lies between birth and 4 months, while cortical myelination continues at least until 6 months. Twelve month-old rats were also studied as a final point of mature myelin status in rodents (Wang et al., 2020). Microstructural changes in rat CC and PFC were analyzed using magnetic resonance imaging (MRI), in parallel with evaluation in tissue of myelin and axonal damage markers. Mitochondrial mass was also estimated as an essential adaptive/stress response designed to maintain the function of demyelinated axons.

2. Materials and methods

2.1. Housing and experimental groups

All animal procedures were performed according to the National Institute of Health Guide for the Care and Use of Laboratory Animals (NIH Publications No. 80–23) revised in 1996. Animals were maintained on a 12 h/12 h inverted light/dark cycle at 22–23 °C and 40–50% humidity with access to food and water *ad libitum*. They were acclimated to this environment for at least one week before being used in the study. A total of 16 primigravid female Wistar rats (200–250 g) were placed in cages at a proportion of 1 female: 1 male per cage and randomly assigned to two groups of 8 couples each. From mating and during the entire course of pregnancy, one group received drinking water containing 3 mg/L sodium arsenite (Sigma-Aldrich, Saint Louis, MO) corresponding to approximately 0.3 to 0.4 mg/kg/day (No Observed Adverse Effect Level for Wistar rat is 0.4–0.9 mg/Kg/day; ATSDR, 2007), and the control group had access to deionized water. Males were retired 10 days after mating, and dams continued receiving arsenite after birth in drinking water throughout the period of lactation. Offspring ($n = 30$ males per group) were weaned at 4 weeks and housed in groups of 6–8 males. Although behavioral and neurochemical arsenic effects have been indistinctly shown in male and female rats (Zarazúa et al., 2010; Martínez et al., 2011; Niño et al., 2018), for this study including 6- and 12-month-old animals, only males were selected given the sex differences reported for adolescent and adult rats in the white matter and PFC (Willing and Juraska, 2015; Markham et al., 2007). The experimental group continued under arsenic exposure in drinking water until sacrifice at 2, 4, 6, or 12 months of age. At each time point, immunohistochemical and histological experiments were performed in 3–4 rats per group, while 4 animals per group were employed for Western blot analysis. Diffusion tensor imaging (DTI) was performed in two rats per group, and the same animals were longitudinally assessed at each time point.

2.2. Histology

2.2.1. Immunohistochemistry

Rats were deeply anesthetized with sodium pentobarbital and perfused through the left cardiac ventricle with 4% paraformaldehyde in 0.1 M phosphate buffer. Fixed brains were removed, kept in paraformaldehyde during 24 h, and embedded in paraffin. Five micrometer coronal slices containing the PFC, CC, and the anterior commissure (Paxinos and Watson, 2007) were mounted in electrocharged slides. For epitope recovery, tissue sections were submerged in Diva Decloaker (Biocare Medical LLC, Concord, CA) solution at 100 °C in a pressure cooker for 3 min. After 15 min with 0.3% hydrogen peroxide (H_2O_2), they were incubated in a humidity chamber at room temperature to block nonspecific background staining (Background Sniper; Biocare Medical), and endogenous biotin and biotin-binding proteins (avidin/biotin blocking kit; Vector Laboratories Inc., Burlingame, CA) were always followed by rinses with TBS-tween. Primary antibodies anti-myelin basic protein (MBP; Santa Cruz Biotechnology Inc., CA; 1:500) or anti non-phosphorylated neurofilaments (SMI-32 Covance; Emeryville, California; 1:200) were incubated overnight at 4 °C. After incubation, a universal biotinylated linked antibody (DAKO, Carpinteria, CA, USA) was incubated for 30 min, followed by streptavidin-HRP complex (DAKO) for 30 min. Sections were developed with diaminobenzidine substrate using the avidin − biotin horseradish peroxidase system (Vector Laboratories Inc., Burlingame, CA). Negative controls consisted of tissue sections treated without the primary antibody. The sections were analyzed with an Olympus microscope equipped with a digital camera (AmScope, Irvine, CA).

2.2.2. Luxol Fast Blue (LFB) staining

To evaluate demyelination in the CC, 3 sections per brain were

acquired. Five micrometer coronal sections were deparaffinized with xylene and rehydrated using decreasing grades of ethanol. Briefly, sections were transferred to LFB solution at 56 °C overnight, rinsed in ethanol and distilled water followed by staining differentiation using lithium carbonate solution (Merck, Germany) for 15 s to distinguish white matter from gray matter (Ríos et al., 2009). Slides were rinsed twice in xylene (Merck) and mounted with Entellan (Merck). Images were obtained with an Olympus microscope equipped with a digital camera (AmScope).

2.3. Image analysis and semi-quantification

A rat brain atlas was used to identify the anatomical location for each of the regions of interest for MBP and LFB. MBP positivity was quantified using Image J software; images were converted to a 256 Gy-level scale (8 bits), and intensity values were obtained using thresholding operations where only pixels within a given range of colour intensity and size were included for analysis. For evaluation of LFB images, 3 sections per animal were selected at 200 × magnification, and the surface area covered with LFB staining was quantified using a densitometric scanning procedure. All the images were calibrated for distance, colour, and area before their analysis.

2.4. Western blot analysis

The left PFC and CC of each animal were collected for protein extraction after dissection. Tissue was homogenized in extraction buffer (sucrose 320 mM, HEPES 10 mM and EDTA 2 mM) supplemented with protease inhibitors, mechanically homogenized, and spun at 12,000 rpm. Protein samples (50 mg) were loaded. Total proteins were separated on a 12% SDS-PAGE gel and transferred onto polyvinylidene difluoride membranes (PVDF). Membranes were blocked with 5% nonfat milk before being incubated (Bio-Rad, Hercules, CA) overnight at 4 °C with primary antibodies against MBP (1:1000; Santa Cruz, Biotechnology Inc., CA), mitochondrial mass (VDAC; 1:1500; Santa Cruz), amyloid protein precursor (APP; 1:1000; Santa Cruz) and β-actin (1:1000; Santa Cruz). β-actin was used as a loading control. After rinsing, membranes were incubated with horseradish peroxidase-conjugated secondary antibodies (1:2500) for 1 h at room temperature. The blots were then visualized using the enhanced chemiluminescence kit (Pierce, Rockford, IL, USA), and signals were detected using medical blue-sensitive X-ray films. The films were digitalized, and the protein intensities were quantified using Image J software.

2.5. Diffusion tensor imaging

All images were acquired at the National Laboratory for Magnetic Resonance Imaging (Institute of Neurobiology, Universidad Nacional Autónoma de México). Imaging was performed with a 7 T Bruker Pharmascan 70/16US imaging system (Pharmascan, Karlsruhe, Germany) using a rat head 2 × 2 array coil, with animals placed in the prone position. Animals were anesthetized during imaging with 1–1.5% inhaled isoflurane, kept over a heating pad and maintained under respiratory and body temperature monitoring. DTI data sets were acquired with a coronal orientation using a segmented echo planar pulse sequence (2 segments); Fiel-of-view = 25.6 × 25.6 mm^2, matrix = 146 × 146 (yielding in-plane resolution of 0.175 mm per side), 25 slices (thickness of 1 mm), TE = 22.91 ms, TR = 2 s, with diffusion sensitization in 64 unique directions, each with b values of 650, 1200, and 2000 s/mm^2 (δ/Δ = 3/9 ms); 5 volumes without diffusion sensitization (*i.e.*, b = 0 s/mm^2) were acquired prior to the diffusion weighted volumes.

2.5.1. Image analysis

All functional analyses were done with MRtrix3 software version 3.0 (https://www.mrtrix.org/). All images were inspected for artifacts, gross motion, and structural abnormalities. Preprocessing of the diffusion weighted imaging data sets included: 1) denoising using a method based on principal component analysis (Veraart et al., 2016), 2) correction for motion and eddy-current induced distortions by registering each volume to the average b = 650 s/mm^2 volume using a linear transformation with 12 degrees of freedom, and 3) correction for intensity inhomogeneities by first estimating the bias field in the average b = 0 s/mm^2 volume using the N4 algorithm (Tustison et al., 2010), which was then used to modulate each volume. The tensor model (Basser et al., 1994) was estimated using an iteratively reweighted linear least squares method for the preprocessed DWI data sets, from which we derived fractional anisotropy (FA), apparent diffusion coefficient (ADC), radial (RD = λ_1) and axial (AD = (λ_2 + λ_3)/2) diffusivity maps. Tensor-derived metrics were extracted from a manually drawn region of interest (ROI) that encompassed the medial portion of the CC (Paxinos and Watson, 2007). The CC volume (mm^3) of each rat was then calculated as the voxel size multiplied by the number of volumes of each voxel in the ROI supplied. Average values per metric per animal were recorded.

2.6. Statistical analysis

Most data had a normal distribution and were expressed as means ± standard deviation. The differences between the means were analyzed using Student's *t*-test or a two-way analysis of variance (ANOVA), followed by Tukey's *post hoc* test analyses to determine the significance of specific comparisons. To determine differences among groups of the MBP intensity in PFC, since the resulting values were not normally distributed, a nonparametric Friedman test followed by Mann–Whitney U pairwise comparisons were performed. To obtain significant differences between groups as large as 2 standard deviations, a level of significance of 0.05 and a 90% power in two-sided tests were considered, and the number of animals per group was equal to or larger than 4. The data were statistically evaluated using GraphPad InStat software version 3.06.

3. Results

3.1. Cortical myelin-deficient axons and increased mitochondrial mass under arsenic exposure

Cortical myelin observed by MBP immunohistochemistry showed a tendency to decrease from young to late adulthood in control animals (Fig. 1B). A similar pattern was observed in arsenic-exposed animals [$F(3, 24) = 2.207$]. While a significantly lower presence of MBP analyzed through immunohistochemistry was found at 2 months [$F(1, 24) = 24.72$; $p < .05$]; Fig. 1B), Western blot data showed a lower myelination status of arsenic-exposed animals at both 2 and 4 months [$F(1, 24) = 141.3$, $^*p < .05$, Fig. 1C and D]. According to the increased energy demand to maintain electric potentials under demyelination, mitochondrial mass in the PFC was significantly greater in the arsenic group than in the control group [$F(1, 24) = 164.8$, $^*p < .05$; $^{**}p < .01$, Fig. 1C and E].

3.2. Severe hypomyelination of the corpus callosum in arsenic-exposed animals

Analysis of CC revealed persistent and considerably lower myelin content in animals exposed to arsenic throughout adulthood. First, MBP immunohistochemistry showed an age-related decrease in the control group at 6 and 12 months of age (Fig. 2A and B), while the arsenic-exposed animals had lower immunopositivity levels at 2, 4, and 6 months of age [$F(1, 24) = 256.1$, $^*p < .05$; Fig. 2B]. Also, myelin presence evidenced by LFB histochemistry revealed a persistent decrease in control animals and lower values in experimental animals at 2, 4, and 6 months [$F(1, 24) = 50.37$; $^*p < .05$; Fig. 2C and D].

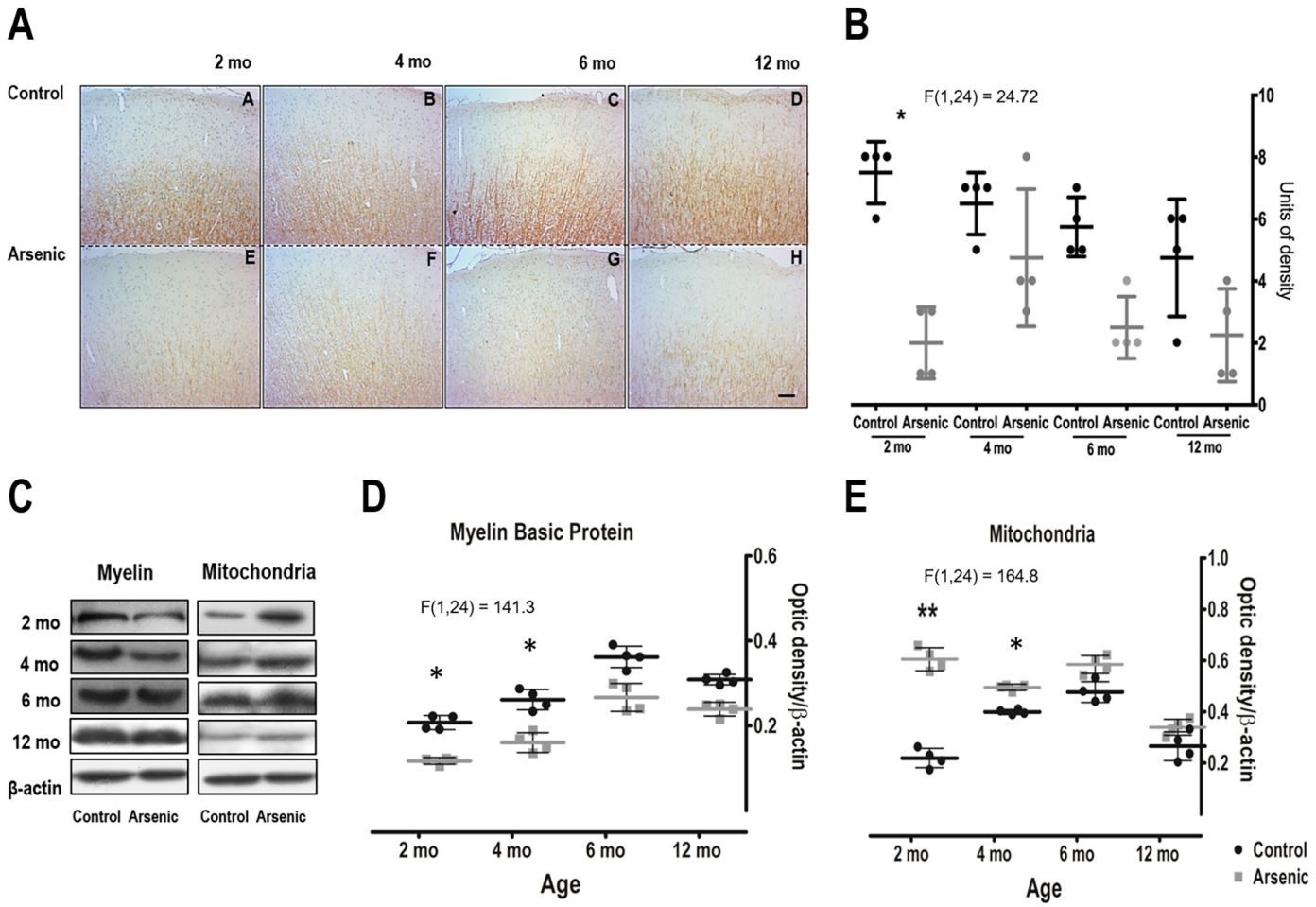

Fig. 1. Cortical myelination and mitochondrial mass are targets of arsenic exposure. A. Cerebral cortex photomicrographs of MBP immunohistochemistry. A-D control group, *E*-H arsenic-exposed group. Original magnification: 200×. B. Quantification of MBP immunopositivity showing a significant effect of arsenic exposure at 2 months of age (*$p < .05$, nonparametric Friedman test). C. Western blot of mitochondrial mass and MBP normalized by β-actin. D and E. Densitometric analysis expressed as mean ± SD of arbitrary units showing significant effects of arsenic exposure at 2 and 4 months of age [F = 164.8, F = 141.3; *p < .05 or **$p < .001$, two-way ANOVA followed by Tukey's *post hoc* test; $n = 4$].

Densitometric measurement of immunoblots demonstrated that MBP content was significantly lower in the arsenic group than in the control group at all time-points studied, Fig. 2F [F (1, 24) = 255.3; *p < .05, **$p < .01$ or ***$p < .001$, two-way ANOVA and Tukey's *post hoc* test; $n = 4$].

3.3. *In vivo longitudinal assessment of the corpus callosum microstructure*

DTI revealed microstructural abnormalities throughout adulthood in the rats exposed to arsenic. Fig. 3A summarizes the *in vivo* differences between the CC from control and arsenic-treated animals at 12 months of age. Diffusion tensors are visualized as ellipses colored according to their orientation, overlaid on the corresponding FA map. Control animals show very elongated diffusion tensors (indicating high FA), as compared to the tensors in the exposed animals (showing low FA). Fig. 3B illustrates the reduced CC volume in the arsenic animals as compared with the controls at all ages. The considerable reductions of FA are due to increased RD, with a concomitant increase of ADC (Fig. 4A-D). Little effect was observed in AD.

3.4. *Axonal damage in fiber tracts under arsenic exposure*

Given that the main differences in myelin were observed in young rats (2 months), axonal damage was examined at this condition through immunohistochemistry against non-phosphorylated neurofilaments and quantification of cortical APP accumulation. The results of this assessment were contrasted with identical tests at 12 months, since in late adulthood the myelination state was similar in arsenic and control groups. The anterior commissure showed similar immunostaining patterns similar to those seen in the CC in both groups, with a slight increase of immunopositivity and irregular tracts at 12 months (Fig. 5A and B). In the PFC, where individual pyramidal neurons can be observed, axons run in a more homogeneous and regular pattern in the control group than in the arsenic group at both ages (Fig. 5C). Axon trajectories in the arsenic group seem tortuous and, in some cases, interrupted. The presence of axonal damage is also suggested by a significant increase of cortical APP at 12 months (*$p < .05$).

4. Discussion

This study provides relevant *in vivo* and *ex vivo* evidence of structural changes and modifications of myelin composition associated with chronic arsenic exposure. Significantly lower levels of MBP immunostaining and LFB staining in the CC together with decreased CC volume measured by MRI demonstrate that the myelin sheath is a target of arsenic. Also, decreased cortical myelination was found accompanied by increased mitochondrial mass. These alterations were present in exposed rats at 2 to 12 months of age, which roughly correspond to adolescence, youth, and adulthood in humans. Connectivity defects caused by these subtle changes in brain white matter certainly

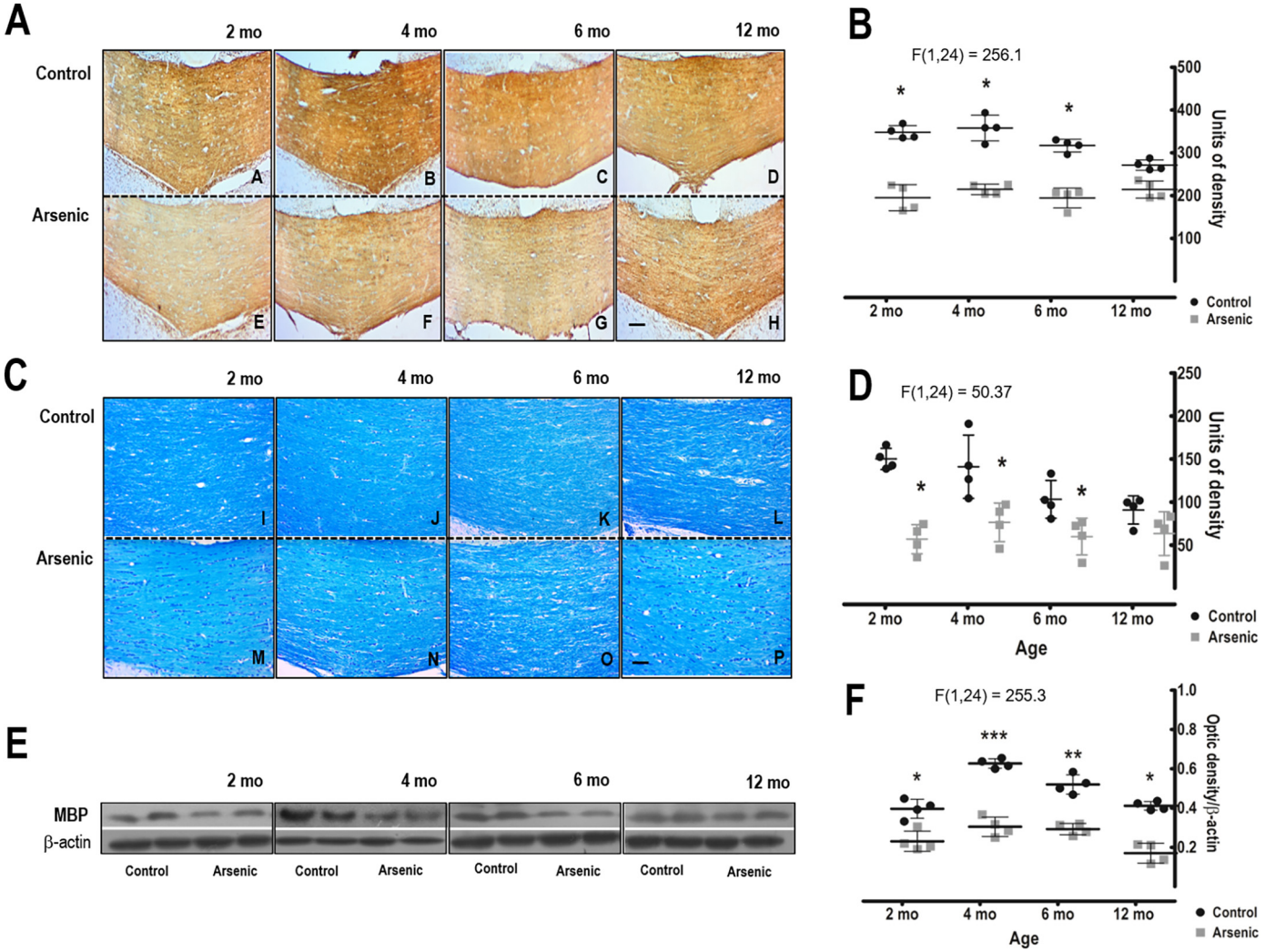

Fig. 2. Severe decrease of myelin levels in the corpus callosum of arsenic-exposed animals. Myelin visualized in the corpus callosum (CC) through MBP immunohistochemistry (light brown, panel A), and in Luxol fast blue (LFB, dense blue, panel C). Original magnification: 200×. B. Comparison of MBP staining of coronal CC in control and arsenic-exposed groups revealing significant demyelination [F = 256.1, *p < .05, two-way ANOVA and Tukey's *post hoc* test]. D. Average LFB demyelination scores (mean ± SD) [F = 50.37, *p < .05]. E. Example MBP immunoblots normalized with β-actin. F. Western blot densitometric analysis showing a lower amount of MBP at all time-points studied associated with arsenic exposure. Data are displayed as arbitrary units and represent mean ± SD [F = 255.3; *p < .05, **p < .01 or ***p < .001, two-way ANOVA and Tukey's *post hoc* test; n = 4]. (For interpretation of the references to colour in this figure legend, the reader is referred to the web version of this article.)

contribute to arsenic-related cognitive deficits observed in animal models and exposed populations. A limitation of these results is that we did not evaluate the effect of arsenic on female rats. The literature suggests that females may be more susceptible to metal neurotoxic effects than males (Llop et al., 2013).In the case of human arsenic studies, poorer mental health was reported in females residing in arsenic affected areas (Syed et al., 2012). Two studies evaluated the neurodevelopment effects in girls by arsenic. One of them found that exposure during prenatal and postnatal periods was inversely related to verbal and full-scale IQ in females (1.5 and 5 years; Hamadani et al., 2011). Signes-Pastor et al., (2019) suggested that exposure to arsenic during pregnancy was related to greater birth length and weight among females. In addition, experimental studies reported hyperactivity in female animals and decreased dopamine presence at wider exposure levels than the same effects in males (Bardullas et al., 2019). Sex differences were also reported in rats when learning deficits associated with the brain cholinergic system were explored (Yadav et al., 2011). Taken together, these reports suggest that it cannot be established whether our findings in males would be similar in female rats. It could be even speculated that the degree of injury in females might be worse than that observed in male rats. Clearly, sex related differences in exposure and health effects caused by arsenic and other substances requiere considerable focus in the future (Singh et al., 2018).

The longitudinal analysis of myelin presence in the PFC and CC, the largest myelinated tract of the brain, allows the observation of the process through two windows. It is clear that demyelination is more evident in the CC whereby myelin formation was mostly completed at 2 months, the first time point analyzed in this work. In this structure, myelin levels seem to remain stable, although at significantly different values between the control and the exposed group along the 12-month observation period. In contrast, we presume that the myelination of intracortical axons is a more dynamic process throughout this period. Arsenic-exposed animals either lack the capacity to build myelin at the same level as control rats or arsenic is attacking the myelin sheaths as they form (Fig. 1B and C). In this context, we interpret the significant increase of mitochondrial mass at 2 months of age as a compensatory reaction to the increased energy demand of chronically demyelinated axons (Fig. 1D). Accordingly, axonal damage is still not observed in these young animals (Fig. 4A). VDAC is a protein abundantly present in the outer mitochondrial membrane, which acts as a co-transporter of

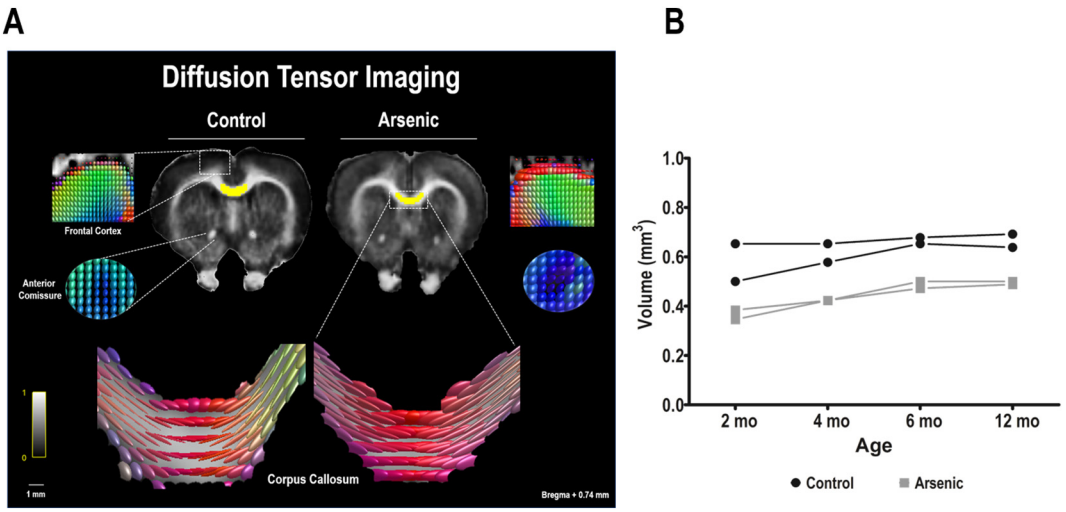

Fig. 3. Tensor diagram and volume decrease of the corpus callosum of arsenic-exposed animals. A. RGB-FA maps of rat brain from 2 months (bottom left) to 12 months (bottom right). FA maps are based on the fiber direction (blue, caudal-rostral; red, left-right; and green, dorsal ventral). Image zoomed into the small ROI shows the diffusion tensor ellipses; brighter colors indicate higher relative anisotropy. B. Comparison of CC volume at all ages tested. (For interpretation of the references to colour in this figure legend, the reader is referred to the web version of this article.)

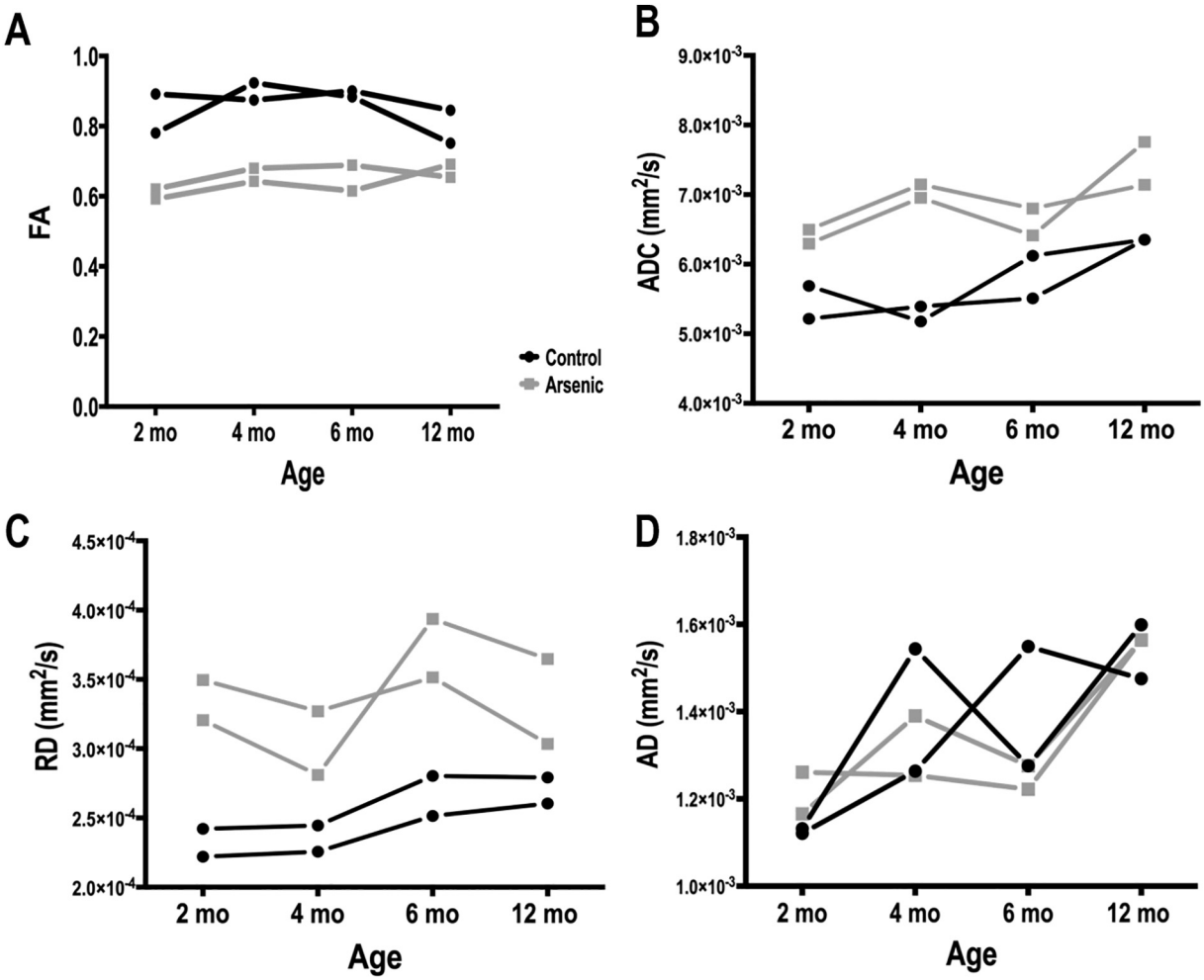

Fig. 4. Trend lines for the evolution of tensor-derived metrics following exposure to arsenic. Comparison of FA, ADC, RD, AD in the middle of the corpus callosum (marked in yellow, Fig. 3) between 2 control and 2 arsenic-exposed animals with repeated follow-up *in vivo* assessments (2, 4, 6, or 12 months). (For interpretation of the references to colour in this figure legend, the reader is referred to the web version of this article.)

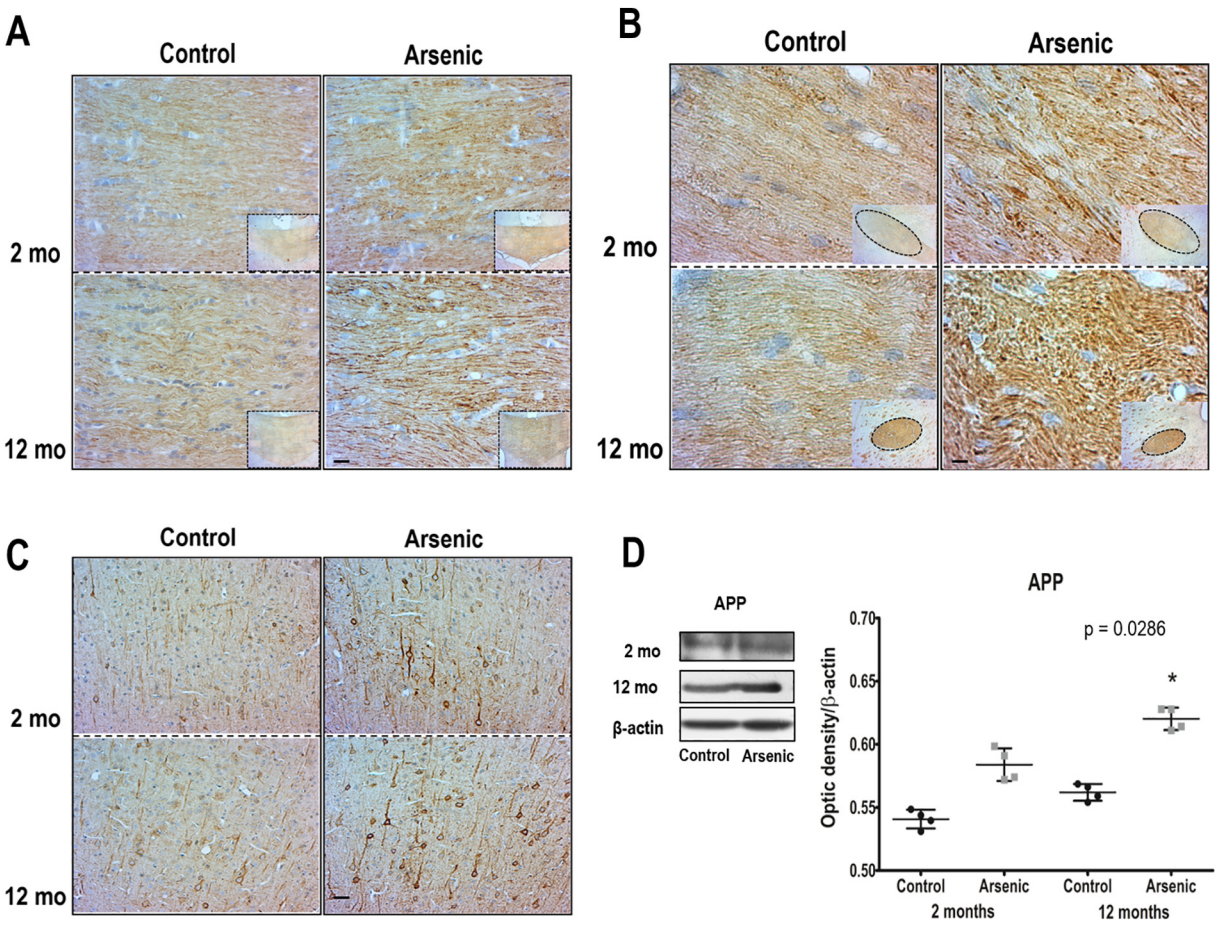

Fig. 5. Increased markers for axonal damage under arsenic exposure. SMI-32 immunopositivity patterns in the corpus callosum (A), anterior commissure (B), and PFC (C) in control and arsenic-exposed rats at 2 and 12 months of age. D. Representative images of Western blot showing the amyloid precursor protein (APP; 110 kDa) in the PFC of the indicated groups. Semi-quantitation of immunoblots analyzed by densitometry; data are presented as arbitrary units and represent mean ± SD, *p < .05 *versus* control, Student's *t*-test.

energy metabolites ATP/ADP (Rostovtseva and Colombini, 1996; Colombini, 1979; Fang and Maldonado, 2018), controlling the efficient energetic cross-talk between mitochondria and the rest of the cell, a critical function for neurons to meet their dynamic energy requirements (Camara et al., 2017). Brain volume is a marker for macroscopic structural changes (Quallo et al., 2009), which is also influenced by the number or diameter of axons (Perge et al., 2012). With these results, it is therefore reasonable to consider that the decreased CC volume (Fig. 3B) is related to the decreased myelin content observed in Fig. 2 and axon diameter. This is the first study that demonstrates a decrease in white matter volume related to arsenic exposure.

Bristow and collaborators demonstrated that axonal mitochondrial enzyme activity is significantly reduced following the developmental myelination of human and rabbit optic nerve tissue (Bristow et al., 2002), indicating that myelinated axons are more energy efficient. Therefore, demyelinated axons would be expected to compensate by upregulating energy production. In this study, the hypomyelination induced by arsenic in the PFC was concomitant with the increased expression of the VDAC at 2–4 months. This compensatory increase, however, was temporary and did not last until 12 months of age. At this time-point, the reduced presence of myelin was further accompanied by axonal damage, revealed by a strong SMI-32 reactivity and APP accumulation (Fig. 5D).

The ability of the PFC to react against the energetic deficit induced by arsenic is also demonstrated in other animal models. Kadeyala et al. observed a significant induction of glutathione-S-transferase (GST) activity in the PFC of PND 21, PND 28, and 3-month-old rats, suggesting a counteracting mechanism adopted to eliminate arsenic (Kadeyala et al., 2013). In a transgenic mouse model exposed to arsenic, the increased presence of antioxidant enzymes allowed a more efficient removal of reactive oxygen species in the PFC than in other brain regions (Niño et al., 2019). Nevertheless, the prolonged energy deficit resulted in both severely reduced ATP levels and protein aggregation. Altogether, these results indicate that increased mitochondrial mass is an adaptation required to maintain/restore conduction in hypomyelinated axons, and strongly suggest that prolonged arsenic exposure disrupts cortical myelination processes despite compensatory cellular responses.

The joint *in vivo* and *ex vivo* findings obtained in the CC also describe a chronic hypomyelination that will certainly lead to defective communication and contribute, together with the observed cortical alterations, to the cognitive deficits associated with chronic arsenic exposure. Myelination of human white matter tracts continues throughout late gestation and after birth in areas such as the hippocampus, PFC, and striatum (Lebel et al., 2012; Gilmore et al., 2018). These structural changes are reflected in an increase in head circumference (Jensen and Holmer, 2018).

Several studies report a reduction of newborn birth weight and head circumference concomitant with high levels of maternal arsenic exposure (Zhong et al., 2019; Wai et al., 2019); also, deficits of cognitive functions in pre-school and school-aged exposed children have been widely demonstrated (Karim et al., 2019). Previous work has shown that arsenic exposure in rats from gestation throughout lactation and development until the age of 4 months alters the morphology of nerve fibers in the corpus striatum and decreases the availability of methyl

groups required for phospholipid synthesis (Ríos et al., 2012; Zarazúa et al., 2010). In addition to the MBP decrease demonstrated by immunohistochemistry and Western blot (Fig. 2), hypomyelination in this study was also confirmed by MRI and DTI analysis.

Measures of DTI likely reflect that both the degree of demyelination and the compactness of the myelin layers contribute to diffusion tensor changes associated with arsenic exposure (Aung et al., 2013b). The lack of significant differences of AD between groups suggests that axons were not severely affected by arsenic exposure, although APP accumulation, a sign of axonal damage, was observed at 12 months of age only in the arsenic group. These findings indicate that myelin itself, or the myelination process, is an arsenic target rather than an aberrant axonal structure. Given that oxidative stress is a core feature of arsenic-exposed models (Mochizuki, 2019), our working hypothesis is that oligodendrocyte precursor cells, which are highly sensitive to oxidative stress, are affected by arsenic, as it has been demonstrated for rats exposed to methyl mercury and for human and rat neural progenitor cells exposed to arsenite (Rai et al., 2013; Masjosthusmann et al., 2019). The potential joint contribution of oligodendrocytes and their precursor cells to this hypomyelination process deserves further examination. In this context, it is important to examine if the initial increase of mitochondrial mass in response to demyelination could also substantially contribute to generating oxidative stress and further compromise oligodendrocyte myelinating functions.

In conclusion, myelin alterations are an important feature of arsenic neurotoxicity. These alterations could be the result of at least three well-demonstrated effects of arsenic, namely oxidative stress, epigenetic alterations, and chemical signaling disturbances. Hypomyelination and poor connectivity, in addition to contributing to cognitive deficit, may lead to neurodegeneration later in life.

Declaration of Competing Interest

The authors declare that they have no known competing financial interests or personal relationships that could have appeared to influence the work reported in this paper.

Acknowledgments

This research was supported by CONACYT (241009) for S.Z. and fellowship 503319 for S.A.N. We thank Leopoldo González-Santos for technical assistant.

References

Andersen, S.L., 2003. Trajectories of brain development: point of vulnerability or window of opportunity? Neurosci. Biobehav. Rev. 27 (1–2), 3–18.
ATSDR, 2007. Agency for toxic substances and disease registry. In: Toxicological Profile for Arsenic. U.S. Department of health and human services.
Aung, K., Kurihara, R., Nakashima, S., Maekawa, F., Nohara, K., Kobayashi, T., Tsukahara, S., 2013a. Inhibition of neurite outgrowth and alteration of cytoskeletal gene expression by sodium arsenite. Neurotoxicology 34, 226–235.
Aung, W.Y., Mar, S., Benzinger, T.L., 2013b. Diffusion tensor MRI as a biomarker in axonal and myelin damage. Imaging Med 5 (5), 427–440.
Bardullas, U., et al., 2009. Chronic low-level arsenic exposure causes gender-specific alterations in locomotor activity, dopaminergic systems, and thioredoxin expression in mice. Toxicol Appl Pharmacol 239 (2), 169–177.
Barkovich, A.J., 2000. Concepts of myelin and myelination in neuroradiology. Am. J. Neuroradiol. 21 (6), 1099–1109.
Basser, P.J., Mattiello, J., LeBihan, D., 1994. MR diffusion tensor spectroscopy and imaging. Biophys. J. 66, 259–267.
Bockhorst, K.H., Narayana, P.A., Liu, R., Ahobila-Vijjula, P., Ramu, J., Kamel, M., Wosik, J., Bockhorst, T., Hahn, K., Hasan, K.M., Perez-Polo, J.R., 2008. Early postnatal development of rat brain: in vivo diffusion tensor imaging. J. Neurosci. Res. 86 (7), 1520–1528.
Bristow, E.A., Griffiths, P.G., Andrews, R.M., Johnson, M.A., Turnbull, D.M., 2002. The distribution of mitochondrial activity in relation to optic nerve structure. Arch. Ophthalmol. 120 (6), 791–796.
Cabral-Pinto, M.M.S., Marinho-Reis, A.P., Almeida, A., Ordens, C.M., Silva, M.M.V.G., Freitas, S., Simões, M.R., Moreira, P.I., Dinis, P.A., Ferreira da Silva, E.A., Condesso de Melo, M.T., 2018. Human predisposition to cognitive impairment and its relation with environmental exposure to potentially toxic elements. Environ. Geochem. Health 40, 1767–1784.
Calderón, J., Navarro, M.E., Jiménez-Capdeville, M.E., Santos-Diaz, M.A., Golden, A., Rodríguez-Leyva, I., Borja-Aburto, V., Díaz-Barriga, F., 2001. Exposure to arsenic and lead and neuropsychological development in Mexican children. Environ. Res. 85, 69–76.
Camara, A.K.S., Zhou, Y., Wen, P.C., Tajkhorshid, E., Kwok, W.M., 2017. Mitochondrial VDAC1: a key gatekeeper as potential therapeutic target. Front. Physiol. 8, 460.
Chandravanshi, L.P., Gupta, R., Shukla, R.K., 2018. Developmental neurotoxicity of arsenic: involvement of oxidative stress and mitochondrial functions. Biol. Trace Elem. Res. 186 (1), 185–198.
Colombini, M., 1979. A candidate for the permeability pathway of the outer mitochondrial membrane. Nature 279, 643–645.
Downes, N., Mullins, P., 2014. The development of myelin in the brain of the juvenile rat. Toxicol. Pathol. 42 (5), 913–922.
Fang, D., Maldonado, E.N., 2018. VDAC regulation: a mitochondrial target to stop cell proliferation. Adv. Cancer Res. 138, 41–69.
Gilmore, J.H., Knickmeyer, R.C., Gao, W., 2018. Imaging structural and functional brain development in early childhood. Nat. Rev. Neurosci. 19 (3), 123–137.
Hamadani, J.D., et al., 2011. Critical windows of exposure for arsenic-associated impairment of cognitive function in pre-school girls and boys: a population-based cohort study. Int J Epidemiol 40 (6), 1593–1604.
Jensen, A., Holmer, B., 2018. White matter damage in 4,725 term-born infants is determined by head circumference at birth: the missing link. Obstet. Gynecol. Int. 28, 2120835.
Jing, J., Zheng, G., Liu, M., Shen, X., Zhao, F., Wang, J., Zhang, J., Huang, G., Dai, P., Chen, Y., Chen, J., Luo, W., 2012. Changes in the synaptic structure of hippocampal neurons and impairment of spatial memory in a rat model caused by chronic arsenite exposure. Neurotoxicology 33, 1230–1238.
Kadeyala, P.K., Sannadi, S., Gottipolu, R.R., 2013. Alterations in apoptotic caspases and antioxidant enzymes in arsenic exposed rat brain regions: reversal effect of essential metals and a chelating agent. Environ. Toxicol. Pharmacol. 36 (3), 1150–1166.
Karim, Y., Siddique, A.E., Hossen, F., Rahman, M., Mondal, V., Banna, H.U., Hasibuzzaman, M.M., Hosen, Z., Islam, M.S., Sarker, M.K., Nikkon, F., Saud, Z.A., Xin, L., Himeno, S., Hossain, K., 2019. Dose-dependent relationships between chronic arsenic exposure and cognitive impairment and serum brain-derived neurotrophic factor. Environ. Int. 131, 105029.
Lebel, C., Gee, M., Camicioli, R., Wieler, M., Martin, W., Beaulieu, C., 2012. Diffusion tensor imaging of white matter tract evolution over the lifespan. NeuroImage 60, 340–352.
Llop, S., Lopez-Espinosa, M.J., Rebagliato, M., et al., 2013. Gender differences in the neurotoxicity of metals in children. Toxicology. 311, 3–12.
Luo, J.H., Qiu, Z.Q., Shu, W.Q., Zhang, Y.Y., et al., 2009. Effects of arsenic exposure from drinking water on spatial memory, ultra-structures and NMDAR gene expression of hippocampus in rats. Toxicol. Lett. 184, 121–125.
Markham, J.A., Morris, J.R., Juraska, J.M., 2007. Neuron number decreases in the rat ventral, but not dorsal, medial prefrontal cortex between adolescence and adulthood. Neuroscience 144, 961–968.
Martínez, L., Jimenez, V., Garcia-Sepulveda, C., Ceballos, F., Delgado, J.M., Niño-Moreno, P., Doniz, L., Saavedra-Alanis, V., Castillo, C.G., Santoyo, M.E., González-Amaro, R., Jiménez-Capdeville, M.E., 2011. Impact of early developmental arsenic exposure on promotor CpG-island methylation of genes involved in neuronal plasticity. Neurochem. Int. 58, 574–581.
Masjosthusmann, S., Siebert, C., Hubenthal, U., Bendt, F., Baumann, J., Fritsche, E., 2019. Arsenite interrupts neurodevelopmental processes of human and rat neural progenitor cells: The role of reactive oxygen species and species-specific antioxidative defense. Chemosphere 235, 447–456.
McKenzie, I.A., Ohayon, D., Li, H., de Faria, J.P., Emery, B., Tohyama, K., Richardson, W.D., 2014. Motor skill learning requires active central myelination. Science 346, 318–322.
Mengler, L., Khmelinskii, A., Diedenhofen, M., Po, C., Staring, M., Lelieveldt, B.P., Hoehn, M., 2014. Brain maturation of the adolescent rat cortex and striatum: changes in volume and myelination. Neuroimage 84, 35–44.
Miller, R.H., 2002. Regulation of oligodendrocyte development in the vertebrate CNS. Prog. Neurobiol. 67, 451–467.
Mochizuki, H., 2019. Arsenic neurotoxicity in humans. Int. J. Mol. Sci. 20 (14), 3418.
Mount, C.W., Monje, M., 2017. Wrapped to adapt: experience-dependent myelination. Neuron 95, 743–756.
Nasrabady, S.E., Rizvi, B., Goldman, J.E., Brickman, A.M., 2018. White matter changes in Alzheimer's disease: a focus on myelin and oligodendrocytes. Acta Neuropathol Commun 6, 22.
Niño, S.A., Martel-Gallegos, G., Castro-Zavala, A., Ortega-Berlanga, B., Delgado, J.M., Hernández-Mendoza, H., Romero-Guzmán, E., Ríos-Lugo, J., Rosales-Mendoza, S., Jiménez-Capdeville, M.E., Zarazúa, S., 2018. Chronic arsenic exposure increases Aβ (1 − 42) production and receptor for advanced glycation end products expression in rat brain. Chem. Res. Toxicol. 31, 13–21.
Niño, S., Morales-Martínez, A., Chi-Ahumada, E., Carrizales, L., Salgado-Delgado, R., Pérez-Severiano, F., Díaz-Cintra, S., Jiménez-Capdeville, M.E., Zarazúa, S., 2019. Arsenic exposure contributes to the bioenergetic damage in an Alzheimer's disease model. ACS Chem. Neurosci. 10, 323–336.
O'Bryant, S.E., Edwards, M., Menon, C.V., Gong, G., Barber, R., 2011. Long-term low-level arsenic exposure is associated with poorer neuropsychological functioning: a project FRONTIER study. Int. J. Environ. Res. Public Health 8, 861–874.
Paus, T., Keshavan, M., Giedd, J.N., 2008. Why do many psychiatric disorders emerge during adolescence? Nat. Rev. Neurosci. 9, 947–957.
Paxinos, G., Watson, C., 2007. The Rat Brain in Stereotaxic Coordinates, 6th Ed. Academic Press, London.

Perge, J.A., Niven, J.E., Mugnaini, E., Balasubramanian, V., Sterling, P., 2012. Why do axons differ in caliber? J. Neurosci. 32 (2), 626–638.
Prayer, D., Barkovich, A.J., Kirschner, D.A., Prayer, L.M., Roberts, T.P., Kucharczyk, J., Moseley, M.E., 2001. Visualization of nonstructural changes in early white matter development on diffusion-weighted MR images: evidence supporting premyelination anisotropy. AJNR Am. J. Neuroradiol. 22 (8), 1572–1576.
Quallo, M.M., Price, C.J., et al., 2009. Gray and white matter changes associated with tool-use learning in macaque monkeys. Proc. Natl. Acad. Sci. U. S. A. 106 (43), 18379–18384.
Rai, N.K., Ashok, A., Rai, A., Tripathi, S., Nagar, G.K., Mitra, K., Bandyopadhyay, S., 2013. Exposure to as cd and Pb-mixture impairs myelin and axon development in rat brain, optic nerve and retina. Toxicol. Appl. Pharmacol. 273 (2), 242–258.
Raz, N., Rodrigue, K.M., 2006. Differential aging of the brain: patterns, cognitive correlates and modifiers. Neurosci. Biobehav. Rev. 30 (6), 730–748.
Ríos, R., Zarazúa, S., Santoyo, M.E., Sepúlveda-Saavedra, J., Romero-Díaz, V., Jiménez, V., Pérez-Severiano, F., Vidal-Cantú, G., Delgado, J.M., Jiménez-Capdeville, M.E., 2009. Decreased nitric oxide markers and morphological changes in the brain of arsenic exposed rats. Toxicology 261 (1 − 2), 68–75.
Ríos, R., Santoyo, M.E., Cruz, D., Delgado, J.M., Zarazúa, S., Jiménez-Capdeville, M.E., 2012. Methyl group balance in brain and liver: role of choline on increased S-adenosyl methionine (SAM) demand by chronic arsenic exposure. Toxicol. Lett. 215, 110–118.
Rostovtseva, T., Colombini, M., 1996. ATP flux is controlled by a voltage-gated channel from the mitochondrial outer membrane. J. Biol. Chem. 271, 28006–28008.
Signes-Pastor, A.J., Doherty, B.T., Romano, M.E., Gleason, K.M., Gui, J., Baker, E., Karagas, M.R., 2019. Prenatal exposure to metal mixture and sex-specific birth outcomes in the New Hampshire Birth Cohort Study. Environmental epidemiology (Philadelphia, Pa.) 3 (5), e068.
Singh, G., Singh, V., Sobolewski, M., Cory-Slechta, D.A., Schneider, J.S., 2018. Sex-Dependent Effects of Developmental Lead Exposure on the Brain. Front. Genet. 9, 89. https://doi.org/10.3389/fgene.2018.00089.
Syed, E.H., et al., 2012. Quality of life and mental health status of arsenic-affected patients in a Bangladeshi population. J Health Popul Nutr 30 (3), 262–269.
Takahashi, N., Sakurai, T., Davis, K.L., Buxbaum, J.D., 2011. Linking oligodendrocyte and myelin dysfunction to neurocircuitry abnormalities in schizophrenia. Prog. Neurobiol. 93, 13–24.
Tsai, S.Y., Chou, H.Y., The, H.W., Chen, C.M., Chen, C., J., 2003. The effects of chronic arsenic exposure from drinking water on the neurobehavioral development in adolescence. Neurotoxicology 24, 747–753.
Tustison, N.J., Avants, B.B., Cook, P.A., Zheng, Y., Egan, A., Yushkevich, P.A., Gee, J.C., 2010. N4ITK: improved N3 Bias correction. IEEE Trans. Med. Imaging 29 (6), 1310–1320.
Tyler, C.R., Allan, A.M., 2014. The effects of arsenic exposure on neurological and cognitive dysfunction in human and rodent studies: a review. Curr Environ Health Rep. 1, 132–147.
Veraart, J., Novikov, D.S., Christiaens, D., Ades-aron, B., Sijbers, J., Fieremans, E., 2016. Denoising of diffusion MRI using random matrix theory. NeuroImage 142, 394–406.
Wai, K.M., Ser, P.H., Ahmad, S.A., Yasmin, R., Ito, Y., Konishi, S., Umezaki, M., Watanabe, C., 2019. In-utero arsenic exposure and growth of infants from birth to 6 months of age: a prospective cohort study in rural Bangladesh. *Int. J. Environ. Health Res.* 29, 1–14.
Wang, F., Ren, S., Chen, J., et al., 2020. Myelin degeneration and diminished myelin renewal contribute to age-related deficits in memory. Nat. Neurosci. https://doi.org/10.1038/s41593-020-0588-8. [Epub ahead of print].
Wasserman, G.A., Liu, X., Loiacono, N.J., Kline, J., Factor-Litvak, P., van Geen, A., Mey, J.L., Levy, D., Abramson, R., Schwartz, A., Graziano, J.H., 2014. A cross-sectional study of well water arsenic and child IQ in Maine schoolchildren. Environ. Health 13, 23–33.
WHO, 2016. Arsenic Fact Sheet. WHO URL. http://www.who.int/es/home.
Willing, J., Juraska, J.M., 2015. The timing of neuronal loss across adolescence in the medial prefrontal cortex of male and female rats. Neuroscience 301, 268–275.
Yadav, R.S., Chandravanshi, L.P., Shukla, R.K., Sankhwar, M.L., Ansari, R.W., Shukla, P.K., Pant, A.B., Khanna, V.K., 2011. Neuroprotective efficacy of curcumin in arsenic induced cholinergic dysfunctions in rats. Neurotoxicology 32, 760–768.
Zarazúa, S., Pérez-Severiano, F., Delgado, J.M., Martínez, L.M., Ortiz-Pérez, D., Jiménez-Capdeville, M.E., 2006. Decreased nitric oxide production in the rat brain after chronic arsenic exposure. Neurochem. Res. 31 (8), 1069–1077. https://doi.org/10.1007/s11064-006-9118-7.
Zarazúa, S., Ríos, R., Delgado, J.M., Santoyo, M.E., Ortiz-Pérez, D., Jiménez-Capdeville, M.E., 2010. Decreased arginine methylation and myelin alterations in arsenic exposed rats. Neurotoxicology 31, 94–100.
Zhong, Q., Cui, Y., Wu, H., Niu, Q., Lu, X., Wang, L., Huang, F., 2019. Association of maternal arsenic exposure with birth size: a systematic review and meta-analysis. Environ. Toxicol. Pharmacol. 69, 129–136.